RSC Advances

PAPER

View Article Online
View Journal | View Issue

Cite this: *RSC Adv.*, 2024, **14**, 35460

In vitro bioactivity, mechanical, and cell interaction of sodium chloride-added calcium sulfate–hydroxyapatite composite bone cements

Pharatree Jaita, [abc] Chamnan Randorn, [d] Anucha Watcharapasorn [ac] and Parkpoom Jarupoom *[ef]

In this research, sodium chloride-added calcium sulfate–hydroxyapatite composite bone cements (0.70CaS–0.30HAP)/*x*NaCl were studied. Different wt% of NaCl (0, 1.5, and 2.5) were added to 0.70CaS–0.30HAP bone cement to investigate the setting time, injectability, washout resistance, phase evolution, physical properties, water absorption, microstructural, chemical analysis, mechanical strength, statistical analysis, *in vitro* apatite-forming ability, and *in vitro* cytotoxicity. With increasing NaCl, the initial setting time decreased to around 3.18 min. X-ray pattern revealed that all composite bone cement samples had mixed phases of CaS, HAP, brushite, gypsum, and NaCl. Water absorption and average grain size increased with increasing NaCl content. The densification and mechanical performances, including σ_c, σ_f, and *E* values, slightly decreased with increasing NaCl content, correlated with the increasing porosity value. This resulted in the production of a porous structure, which caused an excellent *in vitro* apatite-forming ability. The $x = 2.5$ sample showed good bioactivity, inducing the highest apatite mineralization ability in the SBF solution. Additionally, *in vitro* cell culture analysis showed above 94.12% cell viability against a high concentration (@ 200 μg mL^{-1}) for the $x = 2.5$ sample, revealing cytocompatibility. The obtained results indicated that the (0.70CaS–0.30HAP)/2.5NaCl composite bone cement, with good injectability, bioactivity, and cytocompatibility, are promising candidates for biomedical applications.

Received 20th August 2024
Accepted 22nd October 2024

DOI: 10.1039/d4ra06034b

rsc.li/rsc-advances

1 Introduction

Biomaterial bone cements have gained great interest, and are believed to be a promising alternative to traditional sintered bioceramics owing to their self-setting properties, which allow for the direct injection and filling of complicated defect sites.[1,2] Bone cement can be used for filling, bonding, and repairing free-shape defects of bones in dental, orthopedic, and maxillofacial applications *via* minimally invasive procedures.[3] Bone cement can be introduced directly into the defect and conform to its shape, offering enhanced contact with the host tissue. Delivery of the cement paste through a needle or cannula makes it more useful in clinical applications.[2]

Currently, calcium sulfate cement (CSC) is one of the most frequently and intensively studied groups of biomaterial bone cement due to its good biocompatibility and osteoconductivity.[3] CSC possess a long history of clinical use and are known to be a well-tolerated, rapidly and completely bioresorbable material.[2] The ability to set "*in situ*" after filling the defect, the lack of an inflammatory response, and the promotion of bone healing are also the main reasons for this long history.[4] However, some disadvantages of CSC limit their wider clinical applications, including a faster degradation rate than the bone regeneration rate, leading to the formation of many voids in the bone defect after the material is completely degraded. Moreover, CSC resorb too quickly after implantation, which does not match tissue regeneration.[2,4] The other problem is that CSC cannot form a chemical bond with bone tissues in the early stages after implantation due to their poor bioactivity. It is necessary to develop more strategies to slow down the degradation and improve the bioactivity of the CSC.[3,5] Therefore, they are also compounded to perform the composite with other materials such as hydroxyapatite (HAP) to provide favorable resorption characteristics and good bioactivity.

Hydroxyapatite or $Ca_{10}(PO_4)_6(OH)_2$ (HAP), which is the calcium phosphate-based biomaterial,[6] has frequently been

[a]*Department of Physics and Materials Science, Faculty of Science, Chiang Mai University, Chiang Mai 50200, Thailand*

[b]*Office of Research Administration, Chiang Mai University, Chiang Mai 50200, Thailand*

[c]*Center of Excellence in Materials Science and Technology, Materials Science Research Center, Faculty of Science, Chiang Mai University, Chiang Mai 50200, Thailand*

[d]*Department of Chemistry, Faculty of Science, Chiang Mai University, Chiang Mai 50200, Thailand*

[e]*Department of Industrial Engineering, Faculty of Engineering, Rajamangala University of Technology Lanna (RMUTL), Chiang Mai 50300, Thailand. E-mail: noteparkpoom@gmail.com*

[f]*Materials and Medical Innovation Research Unit, Faculty of Engineering, Rajamangala University of Technology Lanna (RMUTL), Chiang Mai 50300, Thailand*

used for bone augmentation since it was discovered that calcium phosphate plays a major role in the inorganic phase of bone, teeth, and hard tissues.[7] Nanohydroxyapatite or *n*HAP stands out as an extensively researched biomaterial in the field of restorative dentistry, as evidenced by studies.[8–10] The HAP is a major component of the inorganic matrix of bones, which comprises approximately 70% of the bone's weight.[11] The HAP can be synthesized by various techniques such as co-precipitation, sol–gel, hydrolysis, combustion, and extraction from the natural (*i.e.* fish bones, shells, chicken eggshells, and bovine bones).[12] The HAP derived from natural sources such as chicken eggshells and bovine bones have demonstrated superior sinterability when compared with their synthetic counterparts in terms of hardness and density. This method is also easy and quick to prepare.[13–15] The HAP has been used extensively as an implant material due to its excellence in biocompatibility and bone-bonding ability. After being implanted into the human body as an artificial material, the HAP can provide scaffolds for the formation of new bone tissues and plays a role in osteoconduction because its calcium and phosphorus can be free from the material surface and absorbed by the body to form new tissues, which have a bone bond with autologous bone tissues.[15–21]

In 2002, the materials containing 60 wt% of HAP (stable component) and 40 wt% of $CaSO_4$ (resorbable component) were developed by Cabaňas *et al.*[4] They reported that the HAP particles act as an element that disturbs the setting reaction, delaying the crystallization of gypsum, increasing the setting time, and decreasing the heat generated during setting of this cement. Moreover, they also found that the biphasic $40CaSO_4$/60HAP showed an improved bioactivity response compared to the pure HAP or single $CaSO_4$ when soaked in a simulated body fluid (SBF) solution. Nilsson *et al.*[18] also reported that the combination of HAP and calcium sulfate (HAP/$CaSO_4$) provides an osteoconductive injectable material with an adequate resorption rate and good mechanical properties. Our preliminary research on hydroxyapatite–calcium sulfate (HAP–*x*CaS) composite bone cement has also indicated that the 0.70CaS–0.30HAP composition has good bioactivity, injectability, and mechanical properties. The 0.70CaS–0.30HAP composite bone cement also produced the highest ability to induce *in vitro* apatite forming. The histological analysis also demonstrated that newer bones are formed around defects and bone cement particles. Osteoblasts were found peripheral at bone trabeculae, and occasional osteoblast-like cells were presented at the granules after 4–8 weeks of implantation.[15]

To better meet clinical requirements for bone defect repair, developing new composite bone cements based on CSC/HAP with ideal degradability and more bioactivity is essential; these cements have been modified with various biologically active cation substitutions. A variety of cationic and anionic substitutions can be attained in apatite minerals.[22] Cao *et al.*[19] studied the sodium chloride-added hydroxyapatite/silk fibroin or NaCl-added HA/SF composites. The results showed that when the content of NaCl was 10 wt%, the scaffolds showed the best mechanical properties, both compressive strengths and modulus. The high-strength NaCl with HA/SF composites may be a potential material in the field of scaffold materials for bone tissue repair. Aguilar *et al.*[21] studied the novel β-TCP scaffold compositions addition with NaCl for bone tissue applications. They reported that the β-TCP + NaCl sample exhibited a porous structure and resulted in higher bioactivity after *in vitro* evaluation on different days and better scaffold dissolution control due to the formation of HAP on the surface. The precipitation of HAP was greater and more homogeneous due to the release of Ca^{2+} and PO_4^{3-} ions that resulted from the dissolution of the porous samples. Those ions led to the formation of nucleation sites of HAP on the surface of the samples. In addition, when NaCl was added, causing a higher concentration of Na^+ and Cl^- ions and increased ionic supersaturation. Tran *et al.*[23] also reported that NaCl was used to fabricate scaffolds with increased interconnectivity, porous microchanneled scaffolds, and multiphasic vascular grafts. When NaCl porogens produced from the nucleation and crystallization methods were incorporated with the traditional salt leaching methods, the interconnectivity was greatly improved. This new generation of porous structures provides great freedom in designing versatile scaffolds with excellent bioactivity for various tissue-engineering applications.

To our knowledge, the (0.70CaS–0.30HAP)/*x*NaCl composite bone cements have not been investigated. Therefore, in this study, we selected the 0.70CaS–0.30HAP composition as the base material due to our preliminary research, which indicated that the composite of 0.70CaS–0.30HAP has good bioactivity, injectability, and mechanical properties.[4,15] A small amount of NaCl was introduced to the 0.70CaS–0.30HAP composite bone cement in varying amounts of 0, 1.5, and 2.5 wt% to increase bioactivity.[21,23] The effect of NaCl on the setting time, injectability, washout resistance, phase, physical, water absorption, microstructural, chemical analysis, mechanical, and statistical analysis was investigated. Moreover, the *in vitro* apatite-forming ability, and *in vitro* cytotoxicity or cell culture analysis are also studied in this work to be tailored over a wide range by changing compositions to meet strict requirements. In this work, we expected that these (0.70CaS–0.30HAP)/*x*NaCl composite bone cement has excellent injectability and biocompatibility with good mechanical performances when compared to a single HAP or CaS or the unmodified 0.70CaS–0.30HAP bone cement, and suggesting their potential in biomedical applications.

2 Experimental

2.1 Synthesis of the hydroxyapatite nano-powder from bovine bone waste using thermal decomposition

In this research, the natural bovine bone, which is a biowaste, is an economical source of hydroxyapatite ($Ca_{10}(PO_4)_6(OH)_2$ or HAP). First, the fresh bones of cows were cut and cleaned well to remove meat and other soft tissues. The bovine bones were boiled for 8 hours in water and were then washed several times to ensure the complete removal of the attached tissue.[7] After that, the boiled bone samples were dried overnight at 120 °C. The deproteinized bones were calcined at 800 °C for 3 h, a temperature at which no prions or any disease-causing agents could survive. The thermally decomposed samples were then

cooled slowly to room temperature (RT) following the procedure of Jaita *et al.*[15,24] Finally, the resulting product was crushed into small pieces by grinding in a mortar. In order to obtain the nano-powder, the HAP powder was milled using a high-energy vibro-milling method for 20 min.

2.2 Preparation of the (0.70CaS–0.30HAP)/*x*NaCl composite bone cement

The HAP nano-powder (derived from the natural bovine bone waste), the medicine grade of calcium sulfate hemihydrate (CSH), and the analytical grade sodium chloride (NaCl) were used as the starting materials. The resulting HAP nano-powder, CSH, and NaCl powders were weighed and mixed to obtain the mixed powder of (0.70CaS–0.30HAP)/*x*NaCl, where $x = 0$, 1.5, and 2.5 wt%. All mixed powders were first tested by XRD to check phase identification. To obtain the composite bone cement, each of the mixed powders was individually mixed with deionized water at a powder-to-liquid ratio of 2 : 1, which was mixed well using a spatula. The mixtures were stirred for 60 s to obtain the homogenous pastes,[1] then quickly transferred to a mold with a rectangular (bar) or cylindrical shape. The (0.70CaS–0.30HAP)/*x*NaCl composite bone cements were placed at 100% humidity and a temperature of 37 °C until the setting steps were completed.[1] After that, all composite bone cements were characterized for their properties. A schematic of methods to prepare the (0.70CaS–0.30HAP)/*x*NaCl composite bone cement with different shapes is shown in Fig. 1.

Fig. 1 Schematic of methods to prepare the (0.70CaS–0.30HAP)/*x*NaCl composite bone cements with different shape.

2.3 Setting time measurements, injectability, and anti-washout tests

Gilmore needle apparatus (ASTM C266-08) was used to determine the prepared cement samples' initial and final setting times.[2] The initial and final setting times were confirmed by the absence of a surface mark using the light and heavy needle. The initial setting time was recorded when the light needle (diameter = 2.12 mm and weight = 113.4 g) penetrated cement less than 1 mm in-depth on the surface of the specimen in three separate areas. The final setting time was defined as the time that elapsed until the heavy needle (diameter = 1.06 mm and weight = 453.6 g) failed to penetrate or produce flaws on the surface of the specimens. The six specimens for each bone cement group were measured, and the results were expressed as mean ± standard deviation (SD).[25–27]

For the injectability test, the cement paste was extruded through a disposable syringe with an inner aperture diameter of 2 mm and injected into Ringer's solution at 37 °C.[28] After that, the weight loss of the cement paste (%) after immersion for 0–30 minutes in the Ringer's solution was measured.[25] Normally, if the cement paste does not dissociate in the Ringer's solution after 30 minutes of immersion and shows the minimum percentage weight loss of cement paste, it is assumed that the cement has passed the anti-washout test.

2.4 Structural analysis

After hardening the composite bone cement for 24 h, the reaction products were examined by X-ray diffractometer (XRD, Rigaku, MiniFlex 600) with CuKα radiation ($\lambda \sim 1.5405$ Å). All samples were characterized by 2θ ranging from 10° to 80° (scanning speed of 0.02° s^{-1}). The quantitative phase composition (%) was analyzed using the SmartLab Studio II program. The quantitative phase analysis was performed and calculated using the reference intensity ratio (RIR) method as shown in eqn (1):[28]

$$\text{RIR}\ (\%) = \frac{\text{intensity of the major peak of the phase}}{\text{sum of intensities of major peaks of all phases}} \times 100\% \quad (1)$$

2.5 Densification and water absorption

In this work, a liquid displacement technique was used to measure the bulk density and porosity measurements. Ethanol was the displacement liquid because the water was the setting liquid. Cement porosity was measured using the Archimedes' principle as described previously.[24,25] Five samples were used for the density and porosity tests. After measuring the dried weight (W_0) of samples, the samples were suspended in ethanol under vacuum for 2 h to make the ethanol infiltrate the pores in the samples. Then, we removed ethanol from the samples' surface and measured the samples' saturated weight (W_1). Finally, the samples' suspended weight (W_2) in ethanol was measured. The porosity of the bone cement was calculated by the following equation:[25,28,29]

$$\text{Porosity}\ (\%) = (W_1 - W_0)/(W_1 - W_2) \times 100\% \quad (2)$$

Furthermore, the linear shrinkage, water absorption, and rate of absorption values were also calculated in this research work.[15]

2.6 Microstructural and chemical analysis

The microstructural analysis of the selected samples was done using a scanning electron microscope (SEM, Prisma E microscope, Thermo Fisher Scientific, USA). The surface was sputter-coated with gold prior to examination with a secondary electron detector at an accelerating voltage of 15 kV and wedge distance of 10 mm.[2] The grain size of all the samples was determined using the linear intercept method (ASTM no. E112-88). The chemical composition of each sample was examined using energy-dispersive X-ray spectroscopy (EDS).

2.7 Mechanical properties

The compressive strength (σ_c) of the cylindrical samples with a size of 5 mm (diameter) × 10 mm (height) was tested on a universal testing machine (Hounsfield, H50KS) at a crosshead speed of 5 mm min^{-1} using a screwdriver load frame.[28] The σ_c of the samples was obtained using the following equation:[15]

$$\sigma_c = \frac{P}{A} \quad (3)$$

where P is the total load on the sample at failure (N) and A is the calculated area of the bearing surface of the sample (mm^2). In this work, the σ_c of each sample after 1, 3, and 7 days of incubation were also measured. The bending strength or flexural strength (σ_f) was also investigated using a universal testing machine (Hounsfield, H50KS) and following the method as described by ASTMC1161-94(1996).[12,30,31] The σ_f of each sample (size 8 × 6 × 100 mm) was determined using the following equation:

$$\sigma_f = \frac{3PL}{2bd^2} \quad (4)$$

where P is the load (force) at the fracture point (N), L is the length of the support span, d is the thickness, and b is the width. In this work, the Young's modulus (E) value was also calculated using the following equation:

$$E = \frac{L^3P}{4bd^3Y} \quad (5)$$

where P is the load (force) at the fracture point (N), L is the length of the support span, d is the thickness, b is the width, and Y is the bending distance of the test sample. The six specimens for each cement group were measured, and the results were expressed as mean ± SD.

2.8 Statistical analysis

For statistical analysis, the statistical difference data was analyzed using a one-way analysis of variance (ANOVA). To find statistical significance, $p < 0.05$ was considered statistically significant using the OriginPro software. Experimental data were processed using Microsoft Excel. The data were presented as the means ± SD.[25–27]

2.9 *In vitro* apatite formation in SBF

All composite bone cements were immersed in the SBF solution to confirm the apatite-forming ability evaluation. The three specimens for each cement group were investigated. The ionic concentration of SBF solution (in mM) was the following: Na^+ = 142.0, K^+ = 5.0, Ca^{2+} = 2.5, Mg^{2+} = 1.5, Cl^- = 148.8, HCO_3^- = 4.2, HPO_4^{2-} = 1.0, SO_4^{2-} = 0.5 (nearly equal to those in human blood plasma).[32,33] The samples were cut into cylindrical shapes of 5 mm in diameter and 10 mm in height and were soaked in SBF at 36.5 °C in a saturated 100% humidity environment. The SBF solution was changed every 1 h for up to 12 h, followed by replacement with fresh solution once a day for 28 days. After 1, 3, 7, 14, and 28 days of soaking in SBF, the samples were investigated for apatite-forming ability by SEM techniques.[24]

2.10 *In vitro* cytotoxicity or cell culture test

The samples' *in vitro* cytotoxicity or the cell culture test was performed using sulforhodamine B (SRB) colorimetric assay for cytotoxicity screening. The human skin fibroblast cell (a primary dermal fibroblast) was cultured in Dulbecco's modified Eagle medium (DMEM) containing 1% penicillin–streptomycin and 10% fetal bovine serum (FBS).[34,35] The cells were plated at a density of 5 × 10^4 cells per mL and cultured in a humidified incubator in an atmosphere containing 5% CO_2 at 37 °C, 95% air, and 100% relative humidity. The control was sodium lauryl sulfate (SLS). The cells were treated at three different concentrations (1, 10, 100, and 200 μg mL^{-1}) of the prepared material. The cell attachment was observed by optical microscope after culturing for 24 h and the average of three readings was counted.[36,37]

3 Results and discussion

3.1 Phase, setting time, injectability, and anti-washout test

X-ray diffraction patterns of the (0.70CaS–0.30HAP)/xNaCl mixed powder, where 2θ = 10–80°, are shown in Fig. 2(a). All compositions had no detectable impurities or secondary peaks in the XRD patterns. The $x = 0$ sample showed mixed CaS (ICDD no. 00-002-0134) and HAP (ICDD no. 00-024-0033) phases. This was also consistent with the previous work.[4] With increasing NaCl content up the $x = 2.5$, the NaCl peak was more observed and marked as "*".

The initial and final setting times as a function of NaCl content are shown in Fig. 2(b), and the related values are also summarized in Table 1. Immediately after mixing the powder and liquid phases, the microstructure of the fresh cement paste begins to develop. The growth and entanglement of the crystals lead to the setting and hardening.[2] Normally, the ratio of liquid to powder, chemical composition, and particle size play a crucial role in the setting time of cement materials. A long setting duration could cause clinical problems due to the cement's inability to maintain shape and support stress during this period.[38] In this research, the initial setting time was further decreased with the increase of NaCl content, and the minimum value of 3.18 ± 0.25 min was found for the $x = 2.5$ sample. The final setting time decreased from 23.65 ± 0.38 min for the $x = 0$ to around 7.79 ± 0.49 min for the $x = 2.5$ sample.

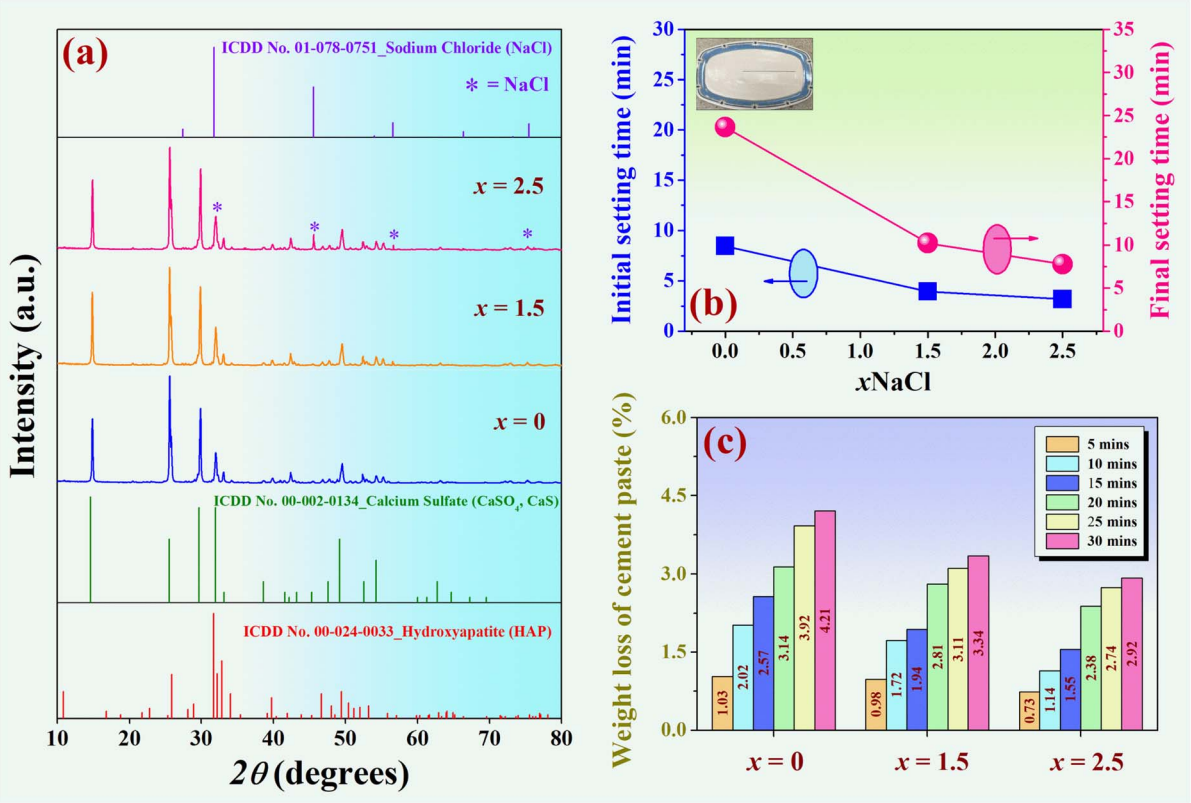

Fig. 2 (a) X-ray diffraction patterns of the (0.70CaS–0.30HAP)/*x*NaCl mixed powder, where $2\theta = 10–80°$, (b) initial setting time and final setting time as a function of NaCl content, and (c) the weight loss of cement paste (%) after immersion in the Ringer's solution as a function of the immersion time.

Table 1 Setting time and physical properties of the (0.70CaS–0.30HAP)/*x*NaCl composite bone cements

x (wt%)	Initial setting time (min)	Final setting time (min)	Weight loss of cement paste[a] (after 30 min immersion) (%)	Density (g cm^{-3})	Porosity (%)	Linkage shrinkage (%)
0	8.44 ± 0.21	23.65 ± 0.38	4.21 ± 1.34	1.31 ± 0.02	44.52 ± 0.07	7.47 ± 0.09
1.5	3.93 ± 0.35	10.19 ± 0.52	3.34 ± 1.04	1.29 ± 0.01	46.61 ± 0.06	7.09 ± 0.05
2.5	3.18 ± 0.25	7.79 ± 0.49	2.92 ± 1.21	1.28 ± 0.01	49.99 ± 0.05	7.01 ± 0.07

[a] Weight loss of cement paste (%) after 30 minutes immersion in the Ringer's solution.

Khairoun *et al.*[39] set a standard for setting time in clinical use: the initial setting time should range from 3 to 8 min, and the final setting time should be less than 15 min. Based on the surgical procedure, an initial setting time of 3 min is preferred for dental applications, whereas an initial setting time of 8 min is desired for orthopedic procedures.[28] The composite bone cement prepared in this study has the initial and final setting times within this recommended range (3.18–7.79 min) to perform the injection comfortably. Therefore, it was also demonstrated that a significant reduction in the setting time would be helpful for clinical procedures.[40,41]

The washout resistance of injected cement was evaluated in this work. Briefly, the cement paste was loaded inside a syringe and injected into Ringer's solution at 37 °C. After 30 min of immersion, the cement paste was considered to pass the washout resistance test if the paste had not disintegrated in the solution.[42] The weight loss of the cement paste (%) after immersion in the Ringer's solution as a function of immersion time is shown in Fig. 2(c), and the related values are also summarized in Table 1. After 30 minutes of immersion, all compositions passed the washout resistance test because the particles did not disintegrate and retained their original shape. However, the $x = 2.5$ sample exhibited a minimum weight loss of cement paste. Therefore, we can conclude that the $x = 2.5$ sample had better injectability because the starch did not dissociate in the solution and could pass the anti-washout test with the minimum weight loss of cement paste value of 2.92 ± 1.21%.

3.2 Phase analysis of the (0.70CaS–0.30HAP)/*x*NaCl composite bone cement

X-ray diffraction patterns of the (0.70CaS–0.30HAP)/*x*NaCl composite bone cement after setting for 24 h at 37 °C and

100% relative humidity,[1] where 2θ = 10–80°, are shown in Fig. 3(a). The XRD result revealed that all composite bone cement samples exhibited the characteristic main peaks of gypsum ($CaSO_4 \cdot 2H_2O$), HAP ($Ca_{10}(PO_4)_6(OH)_2$), dicalcium phosphate dehydrate or brushite (DCPD, $CaHPO_4 \cdot 2H_2O$), a small amount of CaS ($CaSO_4$) and NaCl.[4] Within the detection limits of the XRD instrument, no other impurity or secondary peaks were observed in these XRD patterns. This confirmed the occurrence of no new phase formation. Phase composition (%) was analyzed in-depth by the Reference Intensity Ratio (RIR) method using the SmartLab Studio II program, as shown in Fig. 3(a). The compositions of each phase are also summarized in Table 2. Based on Table 2, the $x = 0$ sample has the mixed phase of gypsum, HAP, brushite, and CaS of 64.43%, 21.89%, 13.64%, and 0.04%, respectively. With increasing NaCl content, the amount of gypsum main phase was found to decrease while the NaCl added phase marked as "*" showed a slight increase (Fig. 3(a)). The $x = 1.5$ sample has the NaCl phase of 4.41%. The NaCl phase was more dominantly observed at 5.11%, especially for the $x = 2.5$ sample. The gypsum in this work was formed by calcium sulfate hemihydrate ($CaSO_4 \cdot 0.5H_2O$) mixed with water. When $CaSO_4 \cdot 0.5H_2O$ reacts with water (H_2O) immediately, it can transform into calcium sulfate dihydrate or gypsum.[43] The chemical process was obtained by the following equation:[2]

Table 2 Phase composition of the (0.70CaS–0.30HAP)/*x*NaCl composite bone cements analyzed by the Reference Intensity Ratio (RIR) method using SmartLab Studio II program

	Phase composition (%)				
x (wt%)	Gypsum	HAP	Brushite	CaS	NaCl
0	64.43	21.89	13.64	0.04	0
1.5	60.57	24.29	10.79	0.21	4.14
2.5	59.69	25.22	9.81	0.17	5.11

$$CaSO_4 \cdot 0.5H_2O + 3H_2O \rightarrow 2CaSO_4 \cdot 2H_2O \quad (6)$$

The setting reaction in the calcium sulfate cement occurs in the following steps: (1) formation of a workable suspension of $CaSO_4 \cdot 0.5H_2O$ and its dissolution, (2) saturation of ions in the aqua solution around $CaSO_4 \cdot 0.5H_2O$ particles, (3) $CaSO_4 \cdot 2H_2O$ precipitation when the supersaturation is achieved, (4) further dissolution of the remaining $CaSO_4 \cdot 0.5H_2O$ as the supersaturation get reduced because of precipitation of $CaSO_4 \cdot 2H_2O$, (5) growth of $CaSO_4 \cdot 2H_2O$ nuclei to larger crystals (secondary nucleation), and (6) interlocking of growing crystals, resulting to the hardening of bone cement.[2] While the formation of brushite as a by-product was possibly thought to result from the

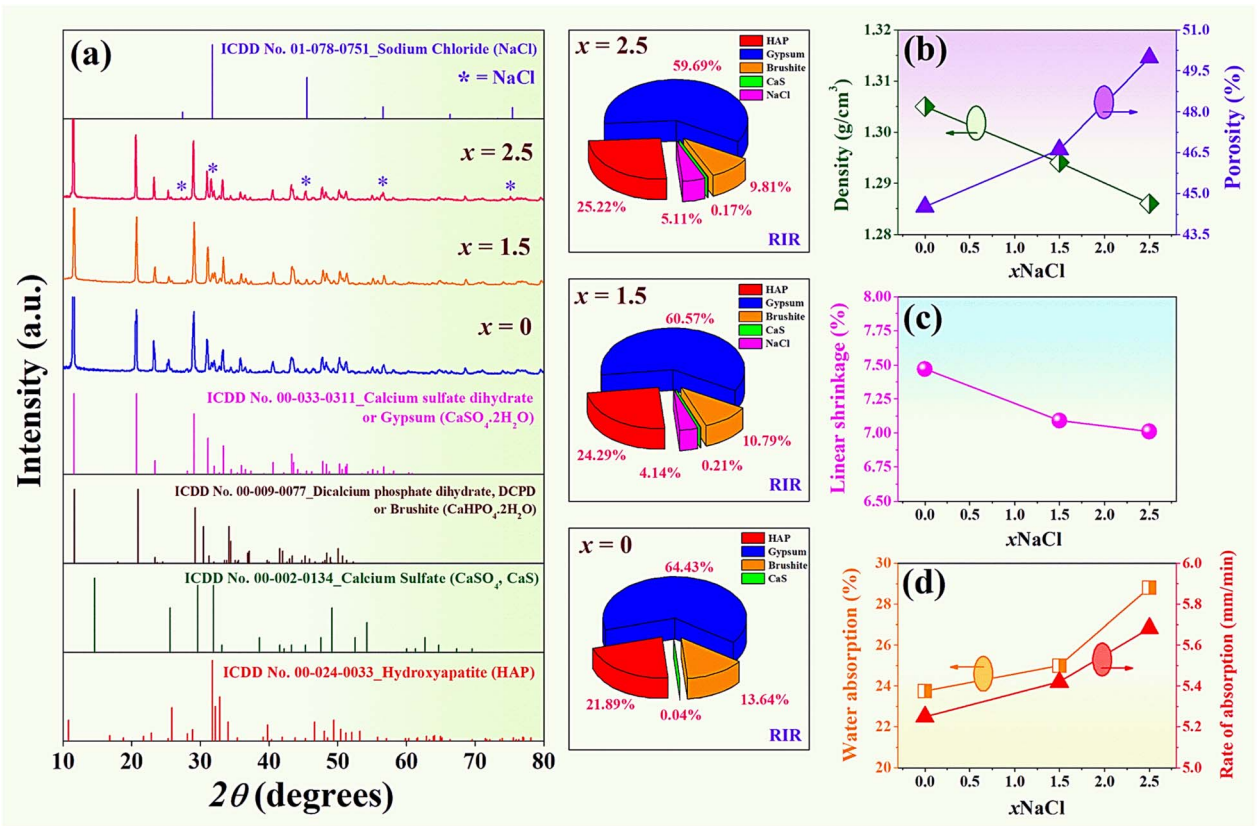

Fig. 3 (a) X-ray diffraction patterns of the (0.70CaS–0.30HAP)/*x*NaCl composite bone cements, where 2θ = 10–80°, and phase composition (%) analyzed by the Reference Intensity Ratio (RIR) method using SmartLab Studio II program, (b) density and porosity as a function of NaCl content, (c) linear shrinkage as a function of NaCl content, and (d) water absorption and rate of absorption as a function of NaCl content.

amount of Ca^{2+} (from $CaSO_4$) and $H_2PO_4^-$ (from $Ca_{10}(PO_4)_6(OH)_2$) ions in the system. In addition, gypsum and brushite cement have high binding properties, which can help improve biological compatibility with living tissues. This was also consistent with the previous works.[43–45]

3.3 Densification and water absorption

Plots of density and porosity as a function of NaCl content of the (0.70CaS–0.30HAP)/*x*NaCl composite bone cement is shown in Fig. 3(b), and the values are listed in Table 1. The data clearly showed that adding NaCl into the 0.70CaS–0.30HAP caused a slight decrease in the samples' density. The density value of the $x = 0$ sample was 1.31 ± 0.02 g cm^{-3}, which was close to 1.294 g cm^{-3} observed earlier by Jaita *et al.* for the HAP–CaS composite bone cement.[15] The density slightly decreased from 1.31 ± 0.02 g cm^{-3} for the $x = 0$ sample to the minimum value of 1.28 ± 0.01 g cm^{-3} for the $x = 2.5$ sample. This result was also correlated with the increase of porosity, as shown in Fig. 3(b), and the reduction of linear shrinkage value with increasing NaCl additive, as shown in Fig. 3(c) and Table 1. Aguilar *et al.*[21] also reported that the increase of porosity above 60% enables bone cells to proliferate, mineralize, and consequently repair or stimulate regeneration at the bone defect's site. Furthermore, the mechanical properties are directly linked to the percentage of porosity and the dissolution behavior of the scaffold in *in vitro* studies, which is essential to keep in mind. The water absorption and rate of absorption as a function of NaCl content are also shown in Fig. 3(d). The water absorption and rate of absorption were found to increase with increasing NaCl concentration. They showed a maximum value of water absorption (28.80 ± 0.09%), and the rate of absorption ($\sim 5.68 \pm 0.02$ mm min^{-1}) for the $x = 2.5$ sample (see Table 3).

3.4 Microstructural and chemical analysis

We used the SEM technique to determine the morphologies of all bone cement samples (after setting for 24 h at 37 °C and 100% relative humidity). SEM micrographs with surface mode of the (0.70CaS–0.30HAP)/*x*NaCl composite bone cements, where $x = 0$–2.5 wt%, are shown in Fig. 4. The SEM micrographs were taken at difference magnifications of 2500× and 5000×.

Table 3 Water absorption, microstructure, and mechanical properties of the (0.70CaS–0.30HAP)/*x*NaCl composite bone cements

x (wt%)	Water absorption (%)	Rate of absorption (mm min^{-1})	Grain size (um)	σ_c (MPa)	σ_f (MPa)	*E* (MPa)
0	23.75 ± 0.11	5.25 ± 0.02	12.44 ± 0.11	7.21 ± 0.17	4.81 ± 0.18	1198.42 ± 5.52
1.5	24.99 ± 0.13	5.42 ± 0.04	15.40 ± 0.06	6.85 ± 0.12	4.42 ± 0.09	1040.91 ± 5.02
2.5	28.80 ± 0.09	5.68 ± 0.02	18.27 ± 0.09	6.68 ± 0.14	4.39 ± 0.08	1025.40 ± 2.03

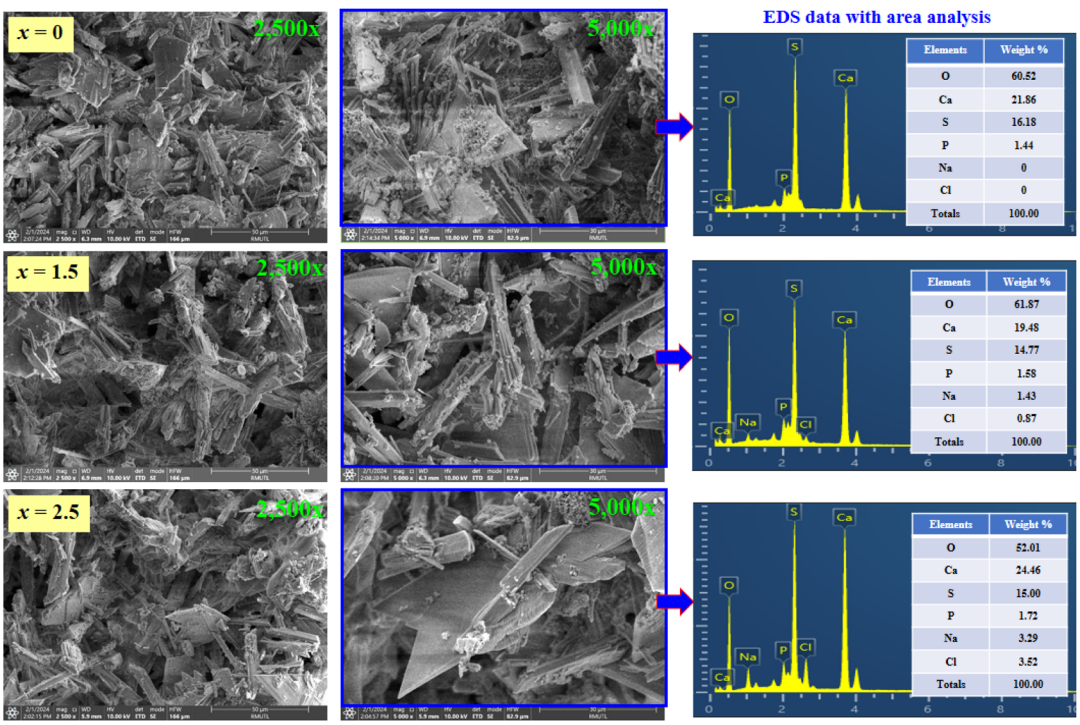

Fig. 4 SEM micrographs with the surface mode (2500× and 5000×) and EDS data with area analysis of the (0.70CaS–0.30HAP)/*x*NaCl composite bone cements, where $x = 0$–2.5 wt%.

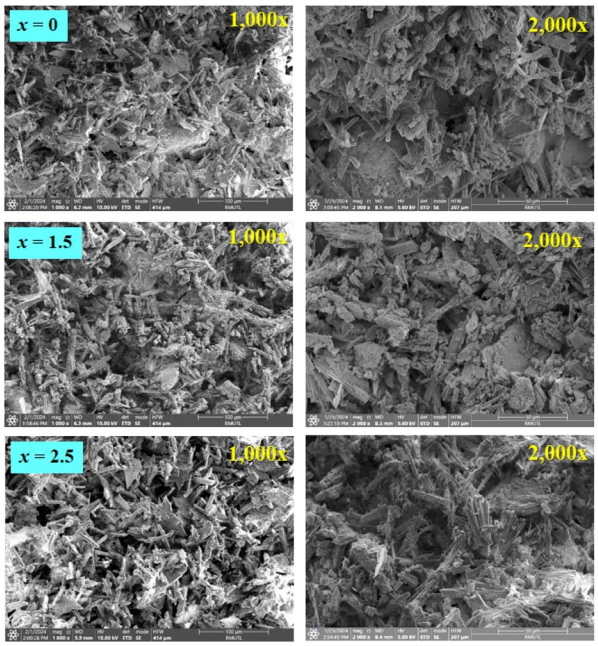

Fig. 5 SEM micrographs with fracture surface mode (1000× and 2000×) of the (0.70CaS–0.30HAP)/*x*NaCl composite bone cements, where $x = 0$–2.5 wt%.

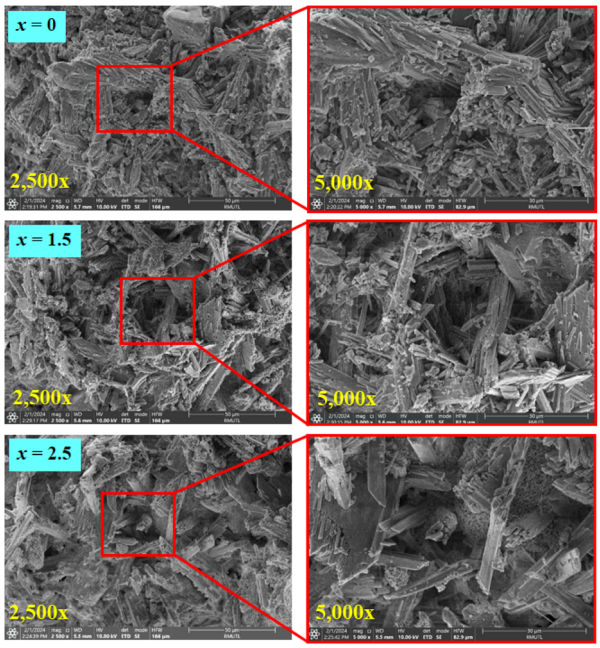

Fig. 6 SEM micrographs with fracture surface mode (2500× and 5000×) of the (0.70CaS–0.30HAP)/*x*NaCl composite bone cements, where $x = 0$–2.5 wt%.

Needle-like shaped and interlocked crystals of CaS attaching HAP agglomerates can be seen from the SEM micrograph.[2] The average grain size values are also summarized in Table 3. The SEM results confirmed that NaCl additive influenced the microstructural and that the average grain size increased with the NaCl modifier concentration. Using the linear intercept method, it was seen that the average grain size increased from 12.44 ± 0.11 μm for the $x = 0$ sample to around 18.27 ± 0.09 μm for the $x = 2.5$ sample, indicating that the NaCl modifier could help to promote grain growth behavior. The EDS data with area mode analysis are also displayed in Fig. 4 (right). The EDS peaks showed that the HAP, CaS, and NaCl were produced successfully. As expected, the weight percent of Na and Cl gradually increased with the amount of NaCl. The maximum weight% of Na (3.29%) and Cl (3.52%) were observed for the $x = 2.5$ sample. This is also well correlated with the observed NaCl peak for this sample in the XRD pattern.

SEM micrographs with fracture surface mode (1000× and 2000× magnification) of the (0.70CaS–0.30HAP)/*x*NaCl composite bone cement, where $x = 0$–2.5 wt% are shown in Fig. 5. The fracture surface of the $x = 0$ sample showed fine grain, denser, and more compact microstructure. The porous structure with more coarse grain was observed with increasing NaCl content. Based on SEM micrographs shown in Fig. 6, it can be seen that the porosity level observed on the fracture surface increased with increasing NaCl content, agreeing well with the slightly decreasing density and increasing porosity values, as seen in Table 1. Tran *et al.*[23] also reported that the resulting NaCl was used to fabricate scaffolds with increased grain growth and more porous structure. When NaCl produced from the nucleation and crystallization methods were incorporated with the traditional salt leaching methods, the interconnectivity was greatly improved. The nucleation techniques to prepare scaffolds with improved interconnectivity with the potential for enhanced cell–cell communication and mass transport played a big role in the overall success of a tissue-engineering scaffold. Pokhrel *et al.*[46] also found that the HAP ceramic derived from bovine bone had many pore structures and resulted in higher porosity. This behavior also produced the porous bone cement structure, which would cause the excellent *in vitro* apatite-forming ability test.[47,48] Moreover, they also reported that the porous structure permitted the sample loading with drugs such as antibiotics or substances that could improve the healing of bone.[46]

3.5 Mechanical properties and statistical analysis

Normally, conventional indentation tests have been widely used to determine the mechanical properties of composite materials,[24] including tensile, hardness, the toughness of bulk materials, bending strength, compressive strength, and elastic modulus.[49] In this work, the mechanical measurements of the synthesized (0.70CaS–0.30HAP)/*x*NaCl composite bone cement were performed through compression tests. The compressive strength (σ_c) and the bending strength (σ_f) were studied using a universal testing machine. The σ_c and σ_f values were calculated using empirical eqn (3) and (4), respectively, and the data are summarized in Table 3. Plots of the σ_c and σ_f values as a function of NaCl content are shown in Fig. 7(a) and (b), respectively. The $x = 0$ sample had the σ_c of 7.21 ± 0.17 MPa and the σ_f of 4.81 ± 0.18 MPa. The σ_c and σ_f values tend to slightly decrease upon increasing the NaCl additive. The $x = 2.5$ sample showed the minimum values of both σ_c (6.68 ± 0.14 MPa) and σ_f

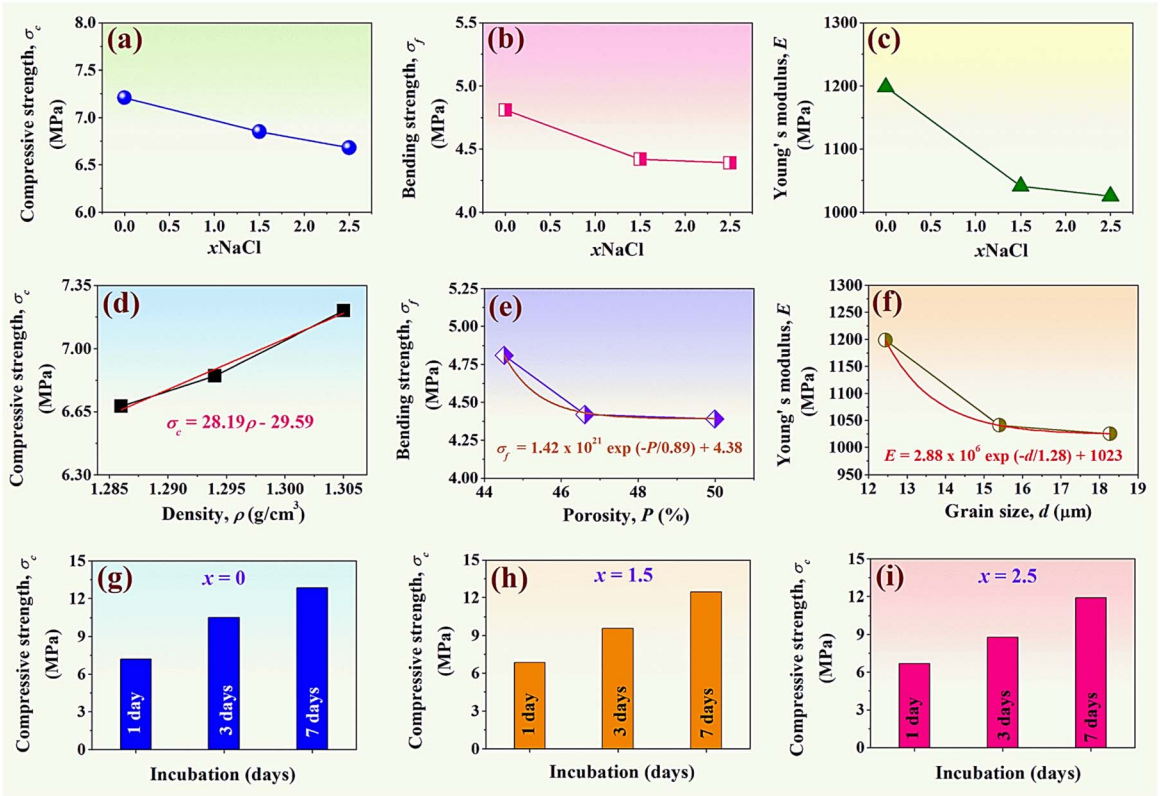

Fig. 7 Plots of (a) σ_c as a function of NaCl content, (b) σ_f as a function of NaCl content, (c) E as a function of NaCl content, (d) σ_c as a function of ρ, (e) σ_f as a function of P, (f) E as a function of d, (g) σ_c as a function of incubation of the $x = 0$ sample, (h) σ_c as a function of incubation of the $x = 1.5$ sample, and (i) σ_c as a function of incubation of the $x = 2.5$ sample.

(4.39 ± 0.08 MPa). The E value was also calculated using empirical eqn (5) and the data are shown in Fig. 7(c). The E value also showed a similar trend to that of σ_c and σ_f. Based on Fig. 7(c), it was found that the E value gradually decreased with increasing NaCl additive. The $x = 2.5$ sample exhibited the minimum value of E (1025.40 ± 2.03 MPa). The slight reduction of mechanical performances with higher NaCl additive concentration was also correlated with the slight reduction of density, decrease of linear shrinkage, and increase of grain size.[50,51] The relationship between the σ_c and the density (ρ) is shown in Fig. 7(d). The σ_c had a linear relation with ρ, which can be expressed as $\sigma_c = 28.19\rho - 29.59$. Statistical analysis showed a significant relationship between the two variables as the P-value in the analysis of variance (ANOVA) indicated that $P = 0.038$, which is lower than 0.05.[52,53] This equation described that one density unit of 28.19 may increase the compressive strength by approximately 29.59. Additionally, analysis of the regression coefficients (R^2) showed that this model can be explain 99.36% of variability in compressive strength. This means a strong relationship exists between these two variables.[53] The σ_f had an exponential relation (first order) with the porosity (P) value, which can be expressed as $\sigma_f = 1.42 \times 10^{21} \exp(-P/0.89) + 4.38$ (see Fig. 7(e)). The analysis of the regression coefficients (R^2) showed that this model can explain 99.75% of variability in bending strength. As expected, a higher porosity volume fraction can result in a lower σ_f value. The E value had an exponential relation (first order) with the grain size (d), which can be expressed as: $E = 2.88 \times 10^6 \exp(-d/1.28) + 1023$ (see Fig. 7(f)). Furthermore, the porosity level evident on the fracture surfaces of the composite bone cement in Fig. 6 was consistent with trends in the measurement of mechanical values.

Plots of the σ_c as a function of incubation (1, 3, and 7 days) of the $x = 0$–2.5 samples are shown in Fig. 7(g)–(i). The initial compressive strength of the composite bone cement samples (@ 1 day) varied between 6.68–7.21 MPa, which is in good agreement with the brushite cement discussed in the previous work (~7.32 MPa).[54] The σ_c of all samples increased with the incubation day, which also correlated with the previous work.[55] After 7 days of incubation, the maximum σ_c value was obtained for all composite bone cements.

Based on the obtained results, it was found that the microstructure correlated with the mechanical performances. The addition of NaCl promoted the porous structure with slightly decreased mechanical performances. This behavior also helps to promote excellent bioactivity, which will be discussed in the next section.

3.6 *In vitro* apatite formation in SBF

Bioactivity is a highly desired feature for the biomaterials intended to be used in bone tissue-engineering applications that have been largely studied in bioactive glasses and glass ceramics. Many studies have assumed that the *in vitro* apatite-

forming ability measured by SBF test and *in vivo* animal models predicts bioactivity. It is widely understood and agreed among researchers that *in vivo* animal models can more accurately predict the performance of biomaterials in the human body. However, *in vivo* animal models are more expensive. Therefore, the *in vitro* apatite-forming ability in SBF can be used for first screening bone bioactive materials before animal testing.[56,57] The SBF solution was first introduced by Kokubo *et al.*[58] to analyze the changes in the surface structure of a bioactive glass ceramic. The SBF test is widely recognized for characterizing the *in vitro* bioactivity of a wide variety of materials. The methods for *in vitro* testing using the SBF immersion test have been recently standardized. The inorganic ion concentration of the SBF solution is nearly equal to that of human blood plasma. The development of SBF is based on the concept that the essential prerequisite to evaluate the bone-binding abilities of a biomaterial is the formation of a bone-like apatite layer on its surface when implanted into the living body. After immersion in the SBF buffer solution (pH = 7.4) for predetermined time points, the resulting layer is evaluated to determine the apatite-forming ability of the tested specimens. The samples are analyzed to identify the formation and growth of all apatites.[56–59]

Concerning the apatite-forming ability evaluation in this work, the (0.70CaS–0.30HAP)/*x*NaCl composite bone cements were immersed in the SBF solution for 1–28 days. Each composite bone cement was limited to 1 cm^2 of the active area and was immersed in falcon tubes containing 40 mL of SBF solution at 37 °C in a water bath.[24] After 1–28 days of soaking in SBF solution, the SEM technique was used to again study each sample. SEM micrographs of the (0.70CaS–0.30HAP)/*x*NaCl composite bone cement after being soaked in SBF solution for 1, 3, 7, 14, and 28 days, where $x = 0$–2.5 wt% are shown in Fig. 8. After immersion in SBF for 1 day, all samples showed a tiny flake (small apatite) deposition on their surface. With the immersion time increasing up to 3 days, more precipitated apatite crystals were observed on the surface of all composite bone cement samples. Furthermore, the formation of the apatite crystals on the surface of all samples significantly increased with increasing NaCl content. A few precipitated apatite crystals were observed on the surface at lower NaCl content ($x = 0$–1.5). However, with increasing NaCl content, the short needle-like apatite crystals were more precipitated and covered the surface, especially for the $x = 2.5$ sample.

After immersion in SBF for 7–14 days, the needle-like apatite crystals were formed more in numbers and were elongated aggregates when compared to those from the 3 day SBF immersions. In addition, the flaky sheet-like structure was also observed. The apatite layer was more precipitated and clearly observed when the immersion time was increased up to 14 days. In addition, the apatite layer was more precipitated and clearly observed with a higher added amount of NaCl. After immersion in the SBF for 28 days, the mixed needle-like and coral-like apatite layer fully covered all surface areas for the $x = 0$ sample. For the $x = 1.5$ sample, the apatite crystals were observed to have a cylindrical shape and clump to form groups with a cactus shape.[48] Especially with the $x = 2.5$ sample after being immersed for 28 days in SBF, the apatite crystals grew to form a cactus shape with a thicker block on the material's surface. Normally, HAP-based material has the ability to promote bone-like apatite formation directly on their surface. The mechanism for the formation of apatite is following: (1) the HAP surface reveals negative surface charges due to the presence of hydroxyl (OH^-) and phosphate (PO_4^{3-}) groups on its surface, (2) these negative ions interact with the positive calcium ions in the SBF to form the Ca-rich ACP or amorphous calcium phosphate, which gain positive surface charge, (3) the

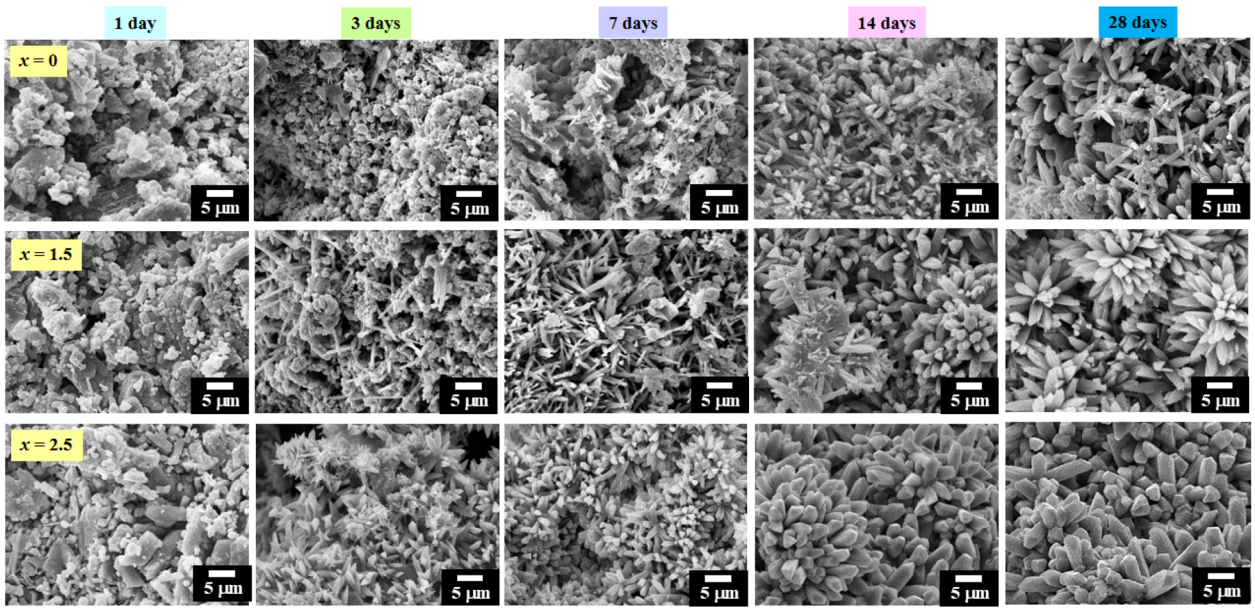

Fig. 8 SEM micrographs of the (0.70CaS–0.30HAP)/*x*NaCl composite bone cements after being soaked in SBF solution for 1, 3, 7, 14, and 28 days, where $x = 0$–2.5 wt%.

Ca-rich ACP interact with the negative phosphate ions in SBF to form the Ca-poor ACP, which stabilizes because of its crystallization into bone-like apatite in the SBF, and (4) nanoscale variations in the surface potential can affect the formation of apatite layer from SBF solution.[60,61]

Based on the above results, it is clearly seen that the incorporation of NaCl during the synthesis procedure of the bone cement sample played a key role in enhancing their surface properties.[56] When NaCl was added into the 0.70CaS–0.30HAP composite bone cement, causing a higher concentration of Na^+ and Cl^- ions (increasing ionic supersaturation). The Cl^- negatively charged surface accumulates Ca^{2+} and the Na^+ positively charged surface accumulates PO_4^{3-}. Those ions led to the formation of nucleation sites for the precipitation of HAP on the surface of the samples and induced the formation of the apatite layer when placed in the SBF due to the increase in viscosity, becoming denser and stickier between the scaffold grains and appearing as small threads on the surface of the samples.[21,60,61] Moreover, the density reduction was observed while the porosity increased with the increase in the NaCl additive. This behavior also produced a porous structure, which caused more precipitated apatite crystals and good *in vitro* apatite-forming ability tests as expected. Therefore, in this research work, the $x = 2.5$ sample exhibited a porous structure with good biocompatibility in the SBF solution.[48,62] The bioactivity of this material is attributed to its compositional and surface characteristics.[48,63] Karageorgiou *et al.*[64] also reported that higher porosity and pore size resulted in greater bone ingrowth with good bioactivity. Liu *et al.*[62] also reported that porous structures are highly desirable because of their high specific surface area, abundant active sites, and surface accessibility. An elevated specific surface area of porous structure can cause a high loading rate, and finally, excellent biocompatibility has been achieved.

3.7 *In vitro* cytotoxicity

In vitro cytotoxicity test is always appealing, due to the lower cost, shorter duration, and higher reproducibility and reliability. The cytotoxicity of a proposed material to a specific cell type can be studied by directly seeding the cells on the material's surface or exposing the cells to the extraction fluid, which falls under an indirect toxicity evaluation. Normally, cytotoxicity assays measure the effects on cells during the first 12–24 hours after exposure to the material.[65] Based on the literature on *in vitro* cytotoxicity, there are various techniques available for conducting the cell viability assay such as sulforhodamine B (SRB), 3-(4,5-dimethylthiazol-2-yl)-2,5-diphenyltetrazolium bromide (MTT), lactate dehydrogenase (LDH), and *etc.*[65] The SRB assay has been widely used to investigate cytotoxicity in cell-based studies and it is the method of choice for the highly cost-effective screenings. The SRB assay is a simple, rapid, inexpensive, and reproducible method for cell density determination, which relies on the binding ability of SRB dye to basic amino-acid residues of cellular proteins, however, its lower sensitivity with non-adherent cells and the need for adding trichloroacetic acid to fix the cells.[34,66–68] MTT and LDH assays monitor the cellular metabolic activity and cell death respectively, based on the reduction of light-absorbing substrates.[65] MTT assay is simple, highly reproducible, and gives a precise dose–response curve on small cell numbers, however, there is no discrimination between cytostatic and cytotoxic effects and

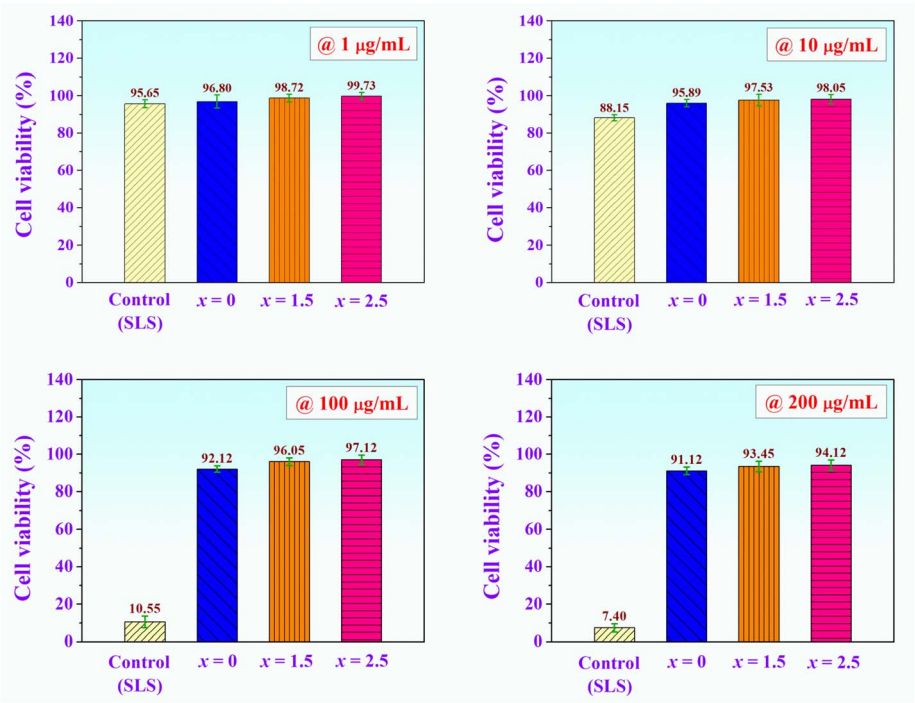

Fig. 9 Plot of cell viability (%) after 24 h of the (0.70CaS–0.30HAP)/*x*NaCl composite bone cements at various concentrations.

can have spectral interferences. LDH assay has a long half-life and can multiplex with any other assay and is fast, however, it is not super sensitive and background contamination *via* animal serum media can occur.[65] However, the *in vitro* cytotoxicity or cell culture test of all composite bone cement samples in this work was performed using SRB assay for cytotoxicity screening due to its user-friendly nature, high reproducibility, and safety considerations.[34,65–68] The plot of cell viability (%) after 24 h of the (0.70CaS–0.30HAP)/*x*NaCl composite bone cement at various concentrations is shown in Fig. 9. According to the cell culture tests at various concentrations from 1 to 200 g mL^{-1}; the results showed no evidence of cytotoxicity. During 24 h of incubation, it was found that the cells proliferated for all samples. Good cell viability was observed. At the higher concentration of 200 μg mL^{-1}, the proliferation of cells was above 91.12–93.45% for $x = 0$–1.5 samples, while the $x = 2.5$ sample had more than 94.12% cell viability. This means that all prepared composite bone cement samples have excellent biocompatibility, particularly the $x = 2.5$ sample.[37,69] Considering *in vitro* cellular activity, it can be confirmed that the $x = 2.5$ sample showed no significant antiproliferative effect after 24 h incubation. No significant morphological changes, non-cytotoxicity, and beneficial for promoting cell growth for these composite bone cements, confirming the biocompatibility, and demonstrating that these composite bone cements are a potential material for bone-related and biomedical applications.[70,71]

4 Conclusions

In this research work, the (0.70CaS–0.30HAP)/*x*NaCl ($x = 0$, 1.5, and 2.5 wt%) composite bone cements were successfully prepared. The setting time, injectability, washout resistance, phase evaluation, physical properties, water absorption, microstructural, chemical analysis, mechanical, statistical analysis, *in vitro* apatite-forming ability, *in vitro* cytotoxicity tests as a function of NaCl added content were performed. The initial setting time and final setting time decreased with increasing NaCl content. The mixed phases of HAP, CaS, brushite, gypsum, and NaCl were found in the XRD pattern. The average grain size increased with increasing NaCl content. The mechanical properties including σ_c, σ_f, and E slightly decreased with increasing NaCl content, which correlated with all composite bone cements exhibiting the porous structure, especially for the $x =$ 2.5. The $x = 2.5$ composite bone cement also produced a higher ability to induce apatite precipitation. The *in vitro* cell culture analysis confirmed the non-cytotoxicity of all compositions to the tested primary dermal fibroblast cells, which means that all prepared bone cement samples are biocompatible and beneficial for promoting cell growth. The above results suggested that the (0.70CaS–0.30HAP)/2.5NaCl composite bone cement has the potential to be a promising material candidate for biomedical applications in the future. In addition, further validation of the *in vitro* cell culture with cancer cells wound healing assays or inflammatory markers, and *in vivo* studies are needed to be performed in the future to confirm the findings of the current study.

Author contributions

Pharatree Jaita: data curation, investigation, methodology, visualization, writing – original draft. Chamnan Randorn: validation, writing – review and editing. Anucha Watcharapasorn: validation, writing – review and editing. Parkpoom Jarupoom: conceptualization, funding acquisition, supervision, writing – review and editing.

Conflicts of interest

The authors declare no conflict of interest.

Acknowledgements

This research project was supported by Fundamental Fund 2024, Chiang Mai University. This research has received funding support from The NSRF *via* the Program Management Unit for Human Resources & Institutional Development, Research and Innovation [B05F640198]. Department of Industrial Engineering, Materials and Medical Innovation Research Unit, Materials and Manufacturing Research Center, Faculty of Engineering, Rajamangala University of Technology Lanna, Department of Physics and Materials Science, Department of Chemistry, Center of Excellence in Materials Science and Technology, Materials Science Research Center, Faculty of Science, and Office of Research Administration, Chiang Mai University are also acknowledged.

References

1 W. Liu, D. Zhai, Z. Huan, C. Wu and J. Chang, Novel tricalcium silicate/magnesium phosphate composite bone cement having high compressive strength, *in vitro* bioactivity and cytocompatibility, *Acta Biomater.*, 2015, **21**, 217–227.
2 A. Zima, J. Czechowsk, D. Siek and A. Ślósarczyk, Influence of magnesium and silver ions on rheological properties of hydroxyapatite/chitosan/calcium sulphate based bone cements, *Ceram. Int.*, 2017, **43**, 16196–16203.
3 F. Hao, L. Qin, J. Liu, J. Chang, Z. Huan and L. Wu, Assessment of calcium sulfate hemihydrate-tricalcium silicate composite for bone healing in a rabbit femoral condyle model, *Mater. Sci. Eng., C*, 2018, **88**, 53–60.
4 M. V. Cabaňas, L. M. R. Lorenzo and M. V. Regí, Setting behavior and *in vitro* bioactivity of hydroxyapatite/calcium sulfate cements, *Chem. Mater.*, 2022, **14**, 3550–3555.
5 G. Yang, J. Liu, F. Li, Z. Pan, X. Ni, Y. Shen, H. Xu and Q. Huang, Bioactive calcium sulfate/magnesium phosphate cement for bone substitute applications, *Mater. Sci. Eng., C*, 2014, **35**, 70–76.
6 W. C. Liu, H. Y. Wang, L. C. Chen, S. W. Huang, C. Wu and R. J. Chung, Hydroxyapatite/tricalcium silicate composites cement derived from novel two-step sol-gel process with good biocompatibility and applications as bone cement and potential coating materials, *Ceram. Int.*, 2019, **45**, 5668–5679.

7 J. K Odusote, Y. Danyuo, A. D Baruwa and A. A. Azeez, Synthesis and characterization of hydroxyapatite from bovine bone for production of dental implants, *J. Appl. Biomater. Funct. Mater.*, 2019, **17**, 1–7.

8 B. S. Karthikeyan and S. Mahalaxmi, Biomimetic dentin remineralization using eggshell derived nanohydroxyapatite with and without carboxymethyl chitosan-An *in vitro* study, *Int. J. Biol. Macromol.*, 2024, **270**, 132359.

9 B. S. Karthikeyan, M. M. Madhubala, G. Rajkumar, V. Dhivya, A. Kishen, N. Srinivasan and S. Mahalaxmi, Physico-chemical and biological characterization of synthetic and eggshell derived nanohydroxyapatite/carboxymethyl chitosan composites for pulp-dentin tissue engineering, *Int. J. Biol. Macromol.*, 2024, **271**, 132620.

10 I. Gurucharan, B. S. Karthikeyan, S. Mahalaxmi, K. Baskar, G. Rajkumar, V. Dhivya, A. Kishen, S. Sankaranarayanan and N. Gurucharan, Characterization of nano-hydroxyapatite incorporated carboxymethyl chitosan composite on human dental pulp stem cells, *Int. Endod. J.*, 2023, **56**, 486–501.

11 A. L. Lesniewicz, P. Szczepanska, M. Kaminska, M. Nowosielska and A. S. Guzend, 6-step manufacturing process of hydroxyapatite filler with specific properties applied for bone cement composites, *Ceram. Int.*, 2022, **48**, 26854–26864.

12 A. Vahdat, B. Ghasemi and M. Yousefpour, Mechanical properties of the hydroxyapatite and magnetic nanocomposite of hydroxyapatite adsorbents, *S. Afr. J. Chem. Eng.*, 2020, **33**, 90–94.

13 S. V. A. Rani, K. Rajkumar, B. S. Karthikeyan, S. Mahalaxmi, G. Rajkumar and V. Dhivya, Micro-Raman spectroscopy analysis of dentin remineralization using eggshell derived nanohydroxyapatite combined with phytosphingosine, *J. Mech. Behav. Biomed. Mater.*, 2023, **141**, 105748.

14 K. Baskar, B. S. Karthikeyan, I. Gurucharan, S. Mahalaxmi, G. Rajkumar, V. Dhivya and A. Kishen, Eggshell derived nano-hydroxyapatite incorporated carboxymethyl chitosan scaffold for dentine regeneration: A laboratory investigation, *Int. Endod. J.*, 2022, **55**, 89–102.

15 P. Jaita, K. Chokethawai, C. Randorn, K. Boonsri, K. Pringproa, K. Thongkorn, A. Watcharapasorn and P. Jarupoom, Enhancing bioactivity and mechanical performances of hydroxyapatite-calcium sulfate bone cements for bone repair: *in vivo* histological evaluation in rabbit femurs, *RSC Adv.*, 2024, **14**, 23286.

16 M. Z. A. Khiri, K. A. Matori, M. H. M. Zaid, C. A. C. Abdullah, N. Zainuddin, I. M. Alibe, N. A. A. Rahman, S. A. A. Wahab, A. Z. K. Azman and N. Effendy, Crystallization behavior of low-cost biphasic hydroxyapatite/β-tricalcium phosphate ceramic at high sintering temperatures derived from high potential calcium waste sources, *Results Phys.*, 2019, **12**, 638–644.

17 W. Yu, X. Wangn, J. Zhaon, Q. Tang, M. Wang and X. Ning, Preparation and mechanical properties of reinforced hydroxyapatite bone cement with nano-ZrO_2, *Ceram. Int.*, 2015, **41**, 10600–10606.

18 M. Nilsson, M. H. Zheng and M. Tägil, The composite of hydroxyapatite and calcium sulphate: a review of preclinical evaluation and clinical applications, *Expert Rev. Med. Devices*, 2013, **10**, 675–684.

19 G. X. Cao, D. Y. Xu, M. Z. Zhou, Z. F. Liao, Y. D. Wang, A novel high strength porous hydroxyapatite/silk fibroin composite: preparation and characterization, *Proceedings of the 2nd Annual International Conference on Advanced Material Engineering (AME 2016)*, 2016.

20 H. Lee, T. S. Jang, J. Song, H. E. Kim and H. D. Jung, The production of porous hydroxyapatite scaffolds with graded porosity by sequential freeze-casting, *Materials*, 2017, **10**, 367.

21 C. R. Aguilar, U. O. Pinto and I. Alfonso, Novel β-TCP scaffold production using NaCl as a porogen for bone tissue applications, *Ceram. Int.*, 2021, **47**, 2244–2254.

22 S. K. Padmanabhan, P. Nitti, E. Stanca, A. Rochira, L. Siculella, M. G. Raucci, M. Madaghiele, A. Licciulli and C. Demitri, Mechanical and biological properties of magnesium- and silicon-substituted hydroxyapatite scaffolds, *Materials*, 2021, **14**, 6942.

23 R. T. Tran, E. Naseri, A. Kolasnikov, X. Bai and J. Yang, A new generation of sodium chloride porogen for tissue engineering, *Biotechnol. Appl. Biochem.*, 2011, **58**, 335–344.

24 P. Jaita and P. Jarupoom, Enhanced magnetic performance and in-vitro apatite-forming ability of the $CoFe_2O_4$ doped nano-hydroxyapatite porous bioceramics, *Microsc. Res. Tech.*, 2023, **86**, 882–897.

25 Y. Xie, J. Liu, S. Cai, X. Bao, Q. Li and G. Xu, Setting characteristics and high compressive strength of an anti-washout, injectable calcium phosphate cement combined with thermosensitive hydrogel, *Materials*, 2020, **13**, 5779.

26 V. H. Arkin, U. Narendrakumar, H. Madhyastha and I. Manjubala, Characterization and *in vitro* evaluations of injectable calcium phosphate cement doped with magnesium and strontium, *ACS Omega*, 2021, **6**, 2477–2486.

27 D. Siek, A. Ślósarczyk, A. Przekora, A. Belcarz, A. Zima, G. Ginalska and J. Czechowska, Evaluation of antibacterial activity and cytocompatibility of α-TCP based bone cements with silver-doped hydroxyapatite and $CaCO_3$, *Ceram. Int.*, 2017, **43**, 13997–14007.

28 U. Tariq, R. Hussain, K. Tufail, Z. Haider, R. Tariq and J. Ali, Injectable dicalcium phosphate bone cement prepared from biphasic calcium phosphate extracted from lamb bone, *Mater. Sci. Eng., C*, 2019, **103**, 109.

29 Y. Shi, L. Yu, C. Gong, W. Li, Y. Zhao and W. Guo, A bioactive magnesium phosphate cement incorporating chondroitin sulfate for bone regeneration, *Biomed. Mater.*, 2021, **16**, 035034.

30 Y. M. Soon, K. H. Shin, Y. H. Koh, J. H. Lee, W. Y. Choi and H. E. Kim, Fabrication and compressive strength of porous hydroxyapatite scaffolds with a functionally graded core/shell structure, *J. Eur. Ceram. Soc.*, 2011, **31**, 13–18.

31 Y. Nie, T. Wang, M. Wu, Y. Qi, W. Wei and Q. Wang, Characterization of a high strength hydroxyapatite cement with dual chelate-setting using phytic acid and citric acid, *Int. J. Appl. Ceram. Technol.*, 2022, **19**, 1498–1510.

32 A. Oyane, K. Onuma, A. Ito, H. M. Kim, T. Kokubo and T. Nakamura, Formation and growth of clusters in conventional and new kinds of simulated body fluids, *J. Biomed. Mater. Res., Part A*, 2003, **64**, 339–348.

33 D. K. Pattanayak, S. Yamaguchi, T. Matsushita, T. Nakamura and T. Kokubo, Apatite-forming ability of titanium in terms of pH of the exposed solution, *J. R. Soc., Interface*, 2012, **9**, 2145–2155.

34 V. Vichai and K. Kirtikara, Sulforhodamine B colorimetric assay for cytotoxicity screening, *Nat. Protoc.*, 2006, **1**, 1113.

35 J. K. Lee, D. B. Kim, J. I. Kim and P. Y. Kim, *In vitro* cytotoxicity tests on cultured human skin fibroblasts to predict skin irritation potential of surfactants, *Toxicol. in Vitro*, 2000, **14**, 345–349.

36 S. Srouji, S. Maurice and E. Livne, Microscopy analysis of bone marrow-derived osteoprogenitor cells cultured on hydrogel 3-D scaffold, *Microsc. Res. Tech.*, 2005, **66**, 132–138.

37 V. R. Sivaperumal, R. Mani, M. S. Nachiappan and K. Arumugam, Direct hydrothermal synthesis of hydroxyapatite/alumina nanocomposite, *Mater. Charact.*, 2017, **134**, 416–421.

38 C. C. Chen, C. W. Wang, N. S. Hsueh and S. J. Ding, Improvement of *in vitro* physicochemical properties and osteogenic activity of calcium sulfate cement for bone repair by dicalcium silicate, *J. Alloys Compd.*, 2014, **585**, 25–31.

39 I. Khairoun, M. G. Boltong, F. C. M. Driessens and J. A. Planell, Effect of calcium carbonate on the compliance of an apatitic calcium phosphate bone cement, *Biomaterials*, 1997, **18**, 1535–1539.

40 W. Zhou, Y. Xue, X. Ji, G. Yin, N. Zhang and Y. Ren, A novel injectable and degradable calcium phosphate/calcium sulfate bone cement, *Afr. J. Biotechnol.*, 2011, **10**, 19449–19457.

41 S. Subramaniam, Y. H. Fang, S. Sivasubramanian, F. H. Lin and C. P. Lin, Hydroxyapatite-calcium sulfate-hyaluronic acid composite encapsulated with collagenase as bone substitute for alveolar bone regeneration, *Biomaterials*, 2016, **74**, 99–108.

42 H. J. Lee, B. Kim, A. R. Padalhin and B. T. Lee, Incorporation of chitosan-alginate complex into injectable calcium phosphate cement system as a bone graft material, *Mater. Sci. Eng., C*, 2019, **94**, 385–392.

43 Z. Pei, Z. Zhang, G. Li, F. Fu, K. Zhang, Y. Cai and Y. Yang, Improvement of *in vitro* osteogenesis and antimicrobial activity of injectable brushite for bone repair by incorporating with Se-loaded calcium phosphate, *Ceram. Int.*, 2021, **47**, 11144–11155.

44 L. Chang, L. Tian, W. Liu and X. Duan, Formation of dicalcium phosphate dihydrate on magnesium alloy by micro-arc oxidation coupled with hydrothermal treatment, *Corros. Sci.*, 2013, **72**, 118–124.

45 V. V. Smirnov, O. S. Antonova, M. A. Goldberg, S. V. Smirnov, L. I. Shvorneva, A. A. Egorov, A. S. Baikin and S. M. Barinov, Bone cements in the calcium phosphate-calcium sulfate system, *Dokl. Chem.*, 2016, **467**, 136–139.

46 S. Pokhrel, Hydroxyapatite: Preparation, properties and its biomedical applications, *Adv. Chem. Eng. Sci.*, 2018, **8**, 225–240.

47 C. Ohtsuki, M. Kamitakahara and T. Miyazaki, Bioactive ceramic-based materials with designed reactivity for bone tissue regeneration, *J. R. Soc., Interface*, 2009, **6**, S349–S360.

48 T. M. T. Dinh, T. T. Nguyen, T. N. Pham, T. P. Nguyen, T. T. T. Nguyen, T. Hoang, D. Grossin, G. Bertrand and C. Drouet, Electrodeposition of HAp coatings on Ti_6Al_4V alloy and its electrochemical behavior in simulated body fluid solution, *Adv. Nat. Sci.: Nanosci. Nanotechnol.*, 2016, **7**, 025008.

49 G. B. Ghorbal, A. Tricoteaux, A. Thuault, G. Louis and D. Chicot, Comparison of conventional knoop and vickers hardness of ceramic materials, *J. Eur. Ceram. Soc.*, 2017, **37**, 2531–2535.

50 A. J. Moulson and J. M. Herbert, *Electroceramics Materials, Properties, Applications*, J. Wiley and Sons, New York, 2nd edn, 2003.

51 P. Jaita and P. Jarupoom, Enhanced dielectric, piezoelectric, and mechanical performances of barium strontium titanate-modified $(Bi_{0.487}Na_{0.487}La_{0.017})TiO_3$ lead-free ceramics, *Integr. Ferroelectr.*, 2021, **213**, 209–220.

52 T. Arahira, M. Maruta and S. Matsuya, Characterization and *in vitro* evaluation of biphasic α-tricalcium phosphate/β-tricalcium phosphate cement, *Mater. Sci. Eng., C*, 2017, **74**, 478–484.

53 S. A. A. Tajudin, M. A. M. Azmi, S. Shahidan, M. H. Z. Abidin and A. Madun, Relationship of physical parameters in Pb-contaminated by stabilization/solidification method, *MATEC Web Conf.*, 2016, **47**, 03015.

54 M. Roy, K. DeVoe, A. Bandyopadhyay and S. Bose, Mechanical and *in vitro* biocompatibility of brushite cement modified by polyethylene glycol, *Mater. Sci. Eng., C*, 2012, **32**, 2145–2152.

55 Z. Ding, W. Xi, M. Ji, H. Chen, Q. Zhang and Y. Yan, Developing a biodegradable tricalcium silicate/gluconodelta-lactone/calcium sulfate dihydrate composite cement with high preliminary mechanical property for bone filling, *Mater. Sci. Eng., C*, 2021, **119**, 111621.

56 Z. V. Osorio, A. Klotschan, M. A. Ospina, Y. Piñeiro, L. Liverani, J. Rivas, M. Michálek, D. Galusek and A. R. Boccaccini, Effect of glycerol and H_3PO_4 on the bioactivity and degradability of rod-like SBA-15 particles with active surface for bone tissue engineering applications, *Microporous Mesoporous Mater.*, 2022, **329**, 111543.

57 A. A. Zadpoor, Relationship between *in vitro* apatite-forming ability measured using simulated body fluid and *in vivo* bioactivity of biomaterials, *Mater. Sci. Eng., C*, 2014, **35**, 134–143.

58 T. Kokubo, H. Kushitani, S. Sakka, T. Kitsugi and T. Yamamuro, Solutions able to reproduce *in vivo* surface-structure changes in bioactive glass-ceramic A-W[3], *J. Biomed. Mater. Res.*, 1990, **24**, 721–734.

59 A. Nouri, R. Castro, J. L. Santos, C. Fernandes, J. Rodrigues and H. Tomás, Calcium phosphate-mediated gene delivery

using simulated body fluid (SBF), *Int. J. Pharm.*, 2012, **434**, 199–208.

60 R. V. Suganthi, S. P. Parthiban, K. Elayaraja, E. K. Girija, P. Kulariya, Y. S. Katharria, F. Singh, K. Asokan, D. Kanjilal and S. N. Kalkura, Investigations on the *in vitro* bioactivity of swift heavy oxygen ion irradiated hydroxyapatite, *J. Mater. Sci.: Mater. Med.*, 2009, **20**, S271–S275.

61 P. Jongwattanapisan, N. Charoenphandhu, N. Krishnamra, J. Thongbunchoo, I. M. Tang, R. Hoonsawat, S. M. Smith and W. Pon-On, *In vitro* study of the SBF and osteoblast-like cells on hydroxyapatite/chitosan-silica nanocomposite, *Mater. Sci. Eng., C*, 2011, **31**, 290–299.

62 S. Liu, X. He, X. Hu, Y. Pu and X. Mao, Porous nanomaterials for biosensing and related biological application in *in vitro*/*vivo* usability, *Mater. Adv.*, 2024, **5**, 453.

63 A. Cahyanto, M. Liemidia, E. Karlina, M. N. Zakaria, K. A. Shariff, C. Sukotjo and A. E. Ghannam, Bioactive carbonate apatite cement with enhanced compressive strength *via* incorporation of silica calcium phosphate composites and calcium hydroxide, *Materials*, 2023, **16**, 2071.

64 V. Karageorgiou and D. Kaplan, Porosity of 3D biomaterial scaffolds and osteogenesis, *Biomaterials*, 2005, **26**, 5474–5491.

65 G. Thrivikraman, G. Madras and B. Basu, *In vitro*/*In vivo* assessment and mechanisms of toxicity of bioceramic materials and its wear particulates, *RSC Adv.*, 2014, **4**, 12763.

66 L. B. Cheol, S. H. Choi and T. S. Kim, Sulforhodamine B assay to determine cytotoxicity of *Vibrio vulnificus* against human intestinal cells, *J. Microbiol. Biotechnol.*, 2004, **14**, 350–355.

67 E. A. Orellana and A. L. Kasinski, Sulforhodamine B (SRB) assay in cell culture to investigate cell proliferation, *Bio-Protoc.*, 2016, **6**, 1–9.

68 M. Papadimitriou, E. Hatzidaki and I. Papasotiriou, Linearity comparison of three colorimetric cytotoxicity assays, *J. Cancer Ther.*, 2019, **10**, 580–590.

69 D. V. Bulajic, J. Drljaca, I. Capo, S. M. Savic, K. Vojisavljevic, A. Hodzic, S. Sekulic and B. V. Bajkin, Biocompatibility of mesoporous SBA-16/hydroxyapatite nanocomposite and dentin demineralized particles on human dental pulp stem cells, *Microsc. Res. Tech.*, 2022, **85**, 1557–1567.

70 M. Precnerová, K. Bodišová, F. Frajkorová, D. Galusková, Z. V. Nováková, J. Vojtaššák, Z. Lenčéš and P. Šajgalík, *In vitro* bioactivity of silicon nitride-hydroxyapatite composites, *Ceram. Int.*, 2015, **41**, 8100–8108.

71 V. R. Sivaperumal, R. Mani, V. Polisetti, K. Aruchamy and T. Oh, Synthesis of hydroxyapatite (HAp)-zirconia nanocomposite powder and evaluation of its biocompatibility: An *in vitro* study, *Appl. Sci.*, 2022, **12**, 11056.